

Photon correlation spectroscopy of light scattered by eye lenses in in vivo conditions

M. Van Laethem,* B. Babusiaux,[†] A. Neetens,[‡] and J. Clauwaert*

*Biophysics Research Group, Department of Biochemistry, University of Antwerp, B-2610 Antwerp; and [†]Department of Ophthalmology, University Hospital Antwerp, B-2520 Antwerp, Belgium

ABSTRACT The application of photon correlation spectroscopy on mammalian eye lenses in vivo is revisited. It is shown that the use of a short wavelength laser type and a logarithmic correlator improves the signal-to-noise ratio to such an extent that shorter measurement times are possible without impairing the information content of the correlation function.

Experimental correlation functions obtained in vivo on a rabbit eye lens, are analyzed with several techniques. The histogram approach is most successful for the determination of the distribution function of relaxation processes in the correlation function and proposes four different populations of components in the lens. This result is comparable to that from in vitro measurements on highly concentrated solutions of α -crystallins and of fiber cell cytoplasm, the former proteins being the main scattering components both in vivo and in vitro in the eye lens system. Our results indicate that the application of photon correlation spectroscopy on eye lenses in vivo offers new perspectives to use this technique as a fast, noninvasive tool to study relaxation phenomena in normal and cataractous lenses. The sensitivity of the method allows it to be used as an important analytical technique in the study of prevention and treatment of cataract.

INTRODUCTION

The eye lens of mammals is a biconvex, avascular, colorless, and almost completely transparent structure, located in the anterior part of the eye behind the pupil-iris diaphragm. The function of the lens is to refract the incoming light in such a way that a sharp image of the environment is formed on the retina. The lens consists of an unusually high fraction of proteins. The concentration of these proteins range from 20% at the outer cortical part to 48% at the central nuclear part of the lens. The remaining part consists of water and a small quantity of ions (Na^+ , K^+), glucose, and some other organic components. The water soluble proteins, called crystallins, form ~90% of the total protein content of the mammalian eye lens. Their presence in the lens has up till now been considered to have a structural and optical role. The overall high concentration of proteins provides a stable structure while the local concentration level contributes to the correct deflection of the incoming light toward the retina.

On a physical, biochemical, and molecular biological basis, three main classes of crystallins can be distinguished in the eye lens of mammals. In order of decreasing molar mass, are the α -crystallins with a molar mass of $\sim 8 \cdot 10^5$ g/mol, the β_H and the β_L crystallins with a molar mass of $2 \cdot 10^5$ and $5 \cdot 10^4$, respectively, and the γ crystallins with a molar mass of $\sim 2 \cdot 10^4$. Their concen-

tration in the lens is 45, 30, 20, and 5% respectively. These data show that the largest crystallins are present in the highest concentration. This will have important consequences for the light scattering behavior of the eye lens as we will see later on.

In spite of its high protein content the eye lens is virtually completely transparent under normal, healthy conditions. A theoretical explanation for this apparent contradiction was given by Benedek in the early seventies (Benedek, 1971) while the experimental confirmation followed much later (Delaye and Tardieu, 1983). Certain types of pathologies reduce the transparency of lens. They induce a partial or total opacification of the lens causing loss of vision, called cataract. On a microscopic scale, opacification is produced by a local heterogeneity in the refractive index of the lens with a minimum extension of half the wavelength of the incoming light; this can be induced by an aggregation of the crystallins or by a drastic local increase or decrease of the concentration of the crystallins. Most of mechanisms that provoke refractive heterogeneities of this size and larger are unknown.

This article is written from the point of view of selecting the conditions for the use of the technique of photon correlation spectroscopy on animal and human lenses; the objective is to use this technique for safe, reliable, and repeatable clinical research and medical diagnostic examination. An example of such a study will be presented at the end of this article.

Address correspondence to Dr. Clauwaert.

THEORY

Photon correlation spectroscopy

The mean scattered intensity per unit volume I_s , in the plane normal to the incident polarization and containing the incident beam, by a dilute solution is given by

$$I_s = I_0 \cdot 4\pi^2 \cdot n^2 \cdot (\partial n/\partial c)^2 \cdot \sin^2 \Theta \cdot M \cdot c/N_A \cdot \lambda^4 \cdot r^2 \cdot n^2, \quad (1)$$

where I_0 is the primary beam intensity, polarized linearly, n is the refractive index of the solution, $(\partial n/\partial c)$ is the refractive index increment of the solute, Θ is the scattering angle, M is the molar mass of the solute, c is the concentration of the solute, N_A is the number of Avogadro, λ is the wavelength in vacuo of the primary beam, and r is the distance from the scattering solution to the detector.

The polarization of the light is considered to be in the vertical plane. In the case of photon correlation spectroscopy (PCS), a laser beam is used as the primary light source. In a homodyne experimental set-up with the particles in pure Brownian motion, the time autocorrelation of the scattered intensity yields the second order or intensity autocorrelation function $G^2(t)$.

In the case of a diluted solution of identical homogeneous spherical particles, small as compared with the wavelength of the incident light, the intensity autocorrelation function has the following form:

$$G^2(t) = A + B \cdot \exp(-2 \cdot D \cdot k^2 \cdot i \cdot \tau), \quad (2)$$

where A is the baseline of the correlation function, B is an experimental constant which depends on the size of the scattering volume and the quality of the optical set-up, D is the translational diffusion coefficient of the scattering particles, k is the scattering vector [$k = 4 \cdot \pi \cdot n \cdot \sin(\Theta/2)/\lambda$], τ is the elementary sample time, and i is the correlator channel number, $i\tau = t$.

The first order or field autocorrelation function $G^1(t)$ is obtained by subtracting the baseline value A from $G^2(t)$ and taking the square root of each channel:

$$G^1(t) = \sqrt{B} \cdot \exp(-D \cdot k^2 \cdot i \cdot \tau). \quad (3)$$

Under the above conditions, $G^1(t)$ takes the form of a pure decaying exponential. The intensity autocorrelation function $G^2(t)$ is usually normalized to $g^2(t)$

$$g^2(t) = 1 + (B/A) \cdot \exp(-2 \cdot D \cdot k^2 \cdot i \cdot \tau). \quad (4)$$

The normalized field autocorrelation function $g^1(t)$ is obtained in a similar way from $G^1(t)$.

In a solution with two discrete size classes of scatterers, the first-order autocorrelation function $g^1(t)$ takes

the form of the sum of two decaying exponentials, each with its own diffusion coefficient D_i and amplitude A_i , $i = 1, 2$. The extension to more than two decaying components is trivial.

When a broad and continuous set of particle sizes is present in the scattering sample, it is assumed that the first-order correlation function can be written as an integral over the relaxation times $\Gamma = D \cdot k^2$:

$$g^{(1)}(k, \tau) = \int F(\Gamma) \cdot \exp(-\Gamma\tau) \cdot d\Gamma. \quad (5)$$

The interesting quantity in Eq. 5 is the distribution function $F(\Gamma)$ which gives the probability that a certain particle size class with relaxation time Γ is present in the scattering volume. The function $F(\Gamma)$ can be considered to be the continuous representation of a large set of discrete amplitudes A_i , each belonging to a certain size class with relaxation time Γ_i . Eq. 5 is also the model used for the first-order correlation function of moderate and highly concentrated solutions of scatterers in Brownian motion.

A number of introductory and advanced textbooks in the field of light scattering and photon correlation spectroscopy are available (Berne and Pecora, 1977; Schulz-Dubois, 1983).

Photon correlation spectroscopy under *in vivo* conditions

Because the aim of this article is to explore the possibilities and limits of PCS for analytical and diagnostic purposes, some attention will be paid on the hardware and software side of this technique.

Choice of the laser light source

The method of PCS has an attractive and for this study necessary feature of being a noninvasive and nondestructive technique. The method will be used for gathering quantitative information about relaxing components in the eye lens of a mammalian. Care has to be taken during a light scattering experiment because the different parts of the eye (e.g., the lens and the retina) may be damaged by the heat generated from the focused laser beam. As the boundary conditions for *in vivo* measurements limit the intensity of laser beam to ~ 15 mW/cm² at the retina (Tanaka and Ishimoto, 1977), one has to look for experimental conditions in which the scattered intensity increases while the primary laser power is kept constant. The He-Ne laser, a standard low cost type of laser for PCS and mostly used in low intensity medical applications, emits light at a wavelength of 632.8 nm; a change to the more rarely used He-Cd laser, emitting at 444 nm, results in an increase of

the scattered intensity by a factor of 4.13 thanks to the inverse fourth power wavelength dependence in Eq. 1.

Since at the same time the refractive index increment ($\partial n / \partial c$) increases by $\sim 8\%$, a further increase of the scattered intensity by a factor of 1.16 can be obtained by switching over to the He-Cd laser. The use of the 363.8 nm line of the Argon ion laser could further improve the situation but only at a substantially higher expense for the laser equipment. The total gain in scattered intensity by using the He-Cd laser over the He-Ne type while keeping all other experimental conditions identical, is calculated to be 4.79. This will increase the signal-to-noise ratio of the recorded correlation function by a factor roughly equal to 2.2. A further important benefit is obtained in the detector section although this depends on the specific detector used. By changing the wavelength from 632.8 to 444 nm, the quantum efficiency of the commonly used S20 cathode increases by a factor of 3 (Thorn Emi Document PMC/86).

The scattering volume remains constant because the focal length of the lenses used and the beam diameter do not appreciably change with λ . The solid angle of coherence, being proportional to λ^2 , is reduced roughly by a factor of 2 on going from 632.8 to 444 nm but this does not impair photon detection in our experimental set-up. In our experimental situation, the angular aperture of the light collection system is much smaller than the coherence solid angle (Chu, 1974) such that the area illuminated on the cathode of the photomultiplier is smaller than one coherence area even at 444 nm. To illustrate the importance of the signal-to-noise ratio of an autocorrelation function for the resolution of the distribution function $F(\Gamma)$, we have simulated an intensity autocorrelation function, resulting from a solution containing two discrete particle size classes with diffusion coefficients $1 \times 10 \exp(-7) \cdot \text{cm}^2 \cdot \text{s}^{-1}$ and $4 \times 10 \exp(-7) \cdot \text{cm}^2 \cdot \text{s}^{-1}$, respectively. The number ratio of both components is chosen such that the scattered intensity is equal for each size class. In the first case a noise level of 0.10% was superimposed on the correlation data, while for the second correlation function a noise level of 0.22% was chosen. The ratio of both noise levels matches the change in scattering cross-section of the situation in which a He-Ne laser is replaced by a He-Cd type as primary light source. For the extraction of the distribution function we have used the program CONTIN (Provencher, 1982).

The distribution function $F(\Gamma)$, calculated from both noise distorted correlation functions, is shown in Fig. 1. The figure shows clearly that only in the case of the lower noise level the distribution function is resolved into two components, positioned at the correct values compared with the simulation. The distribution function, calculated from the correlation function with the

higher noise level, only shows an unclear trace of a second population of scattering particles by the shoulder in the broad peak but no reliable numerical values for both the diffusion coefficients and their relative amplitude can be obtained.

Correlators

It has been shown that concentrated solutions of proteins *in vitro* give rise to slowly decaying components in the intensity autocorrelation function of a laser light scattering experiment. For bovine eye cytoplasm, relaxation times up to 10 ms have been identified (Delaye et al., 1982). For concentrated solutions of α -crystallin it has been shown that the correlation function contains components with relaxation times of 100 and 1,000 ms at a scattering angle of 90° (Licinio et al., 1987). These extremely long time constants correspond to diffusion coefficients of $1.7 \times 10 \exp(-10) \text{ cm}^2 \text{s}^{-1}$ and $1.7 \times 10 \exp(-11) \text{ cm}^2 \text{s}^{-1}$, respectively. Suppose we want to study the dynamics of a solution containing a bimodal solution of monodisperse scattering particles. The diffusion coefficients of each size class are $1 \times 10 \exp(-7) \text{ cm}^2 \text{s}^{-1}$ and $1 \times 10 \exp(-10) \text{ cm}^2 \text{s}^{-1}$. The correlator we have at our disposal has 128 linearly spaced channels. This allows us to calculate the sample time τ we must choose to cover the entire relaxation decay of the correlation function, reaching to ~ 100 ms. At a scattering angle of 130°, the sample time turns out to be 4.77 ms. This long sample time is entirely due to the presence of the slow decaying component. With such a value of τ , the resolution of the initial decay of the correlation function is very low. It is easily calculated that the fast component has died out completely within the period of the first two sample times. We can, however, take advantage of the steady development in the concepts of correlator building since the appearance of the linearly spaced correlator. One type of commercially available correlator allows the experimenter to record four correlation functions simultaneously, each with a different sample time. The channels of each of the separate correlators are linearly spaced while the ratio of the first channels form a geometric series with ratio 4. For such a correlator containing $4 \times 32 = 128$ channels, it is easily calculated that a sample time of 0.30 ms has to be selected for the first correlator to cover the same range in relaxation times. We now get information about the behavior of the decay of the correlation on four different time scales with sample times 0.30, 1.19, 4.77, and 19.1 ms but the resolution of the initial decay remains poor. Moreover, due to the peculiar hardware construction of the correlator, some ambiguity is introduced on the data since the four correlograms, although recorded simultaneously, do not match perfectly.

The most interesting solution comes from a new

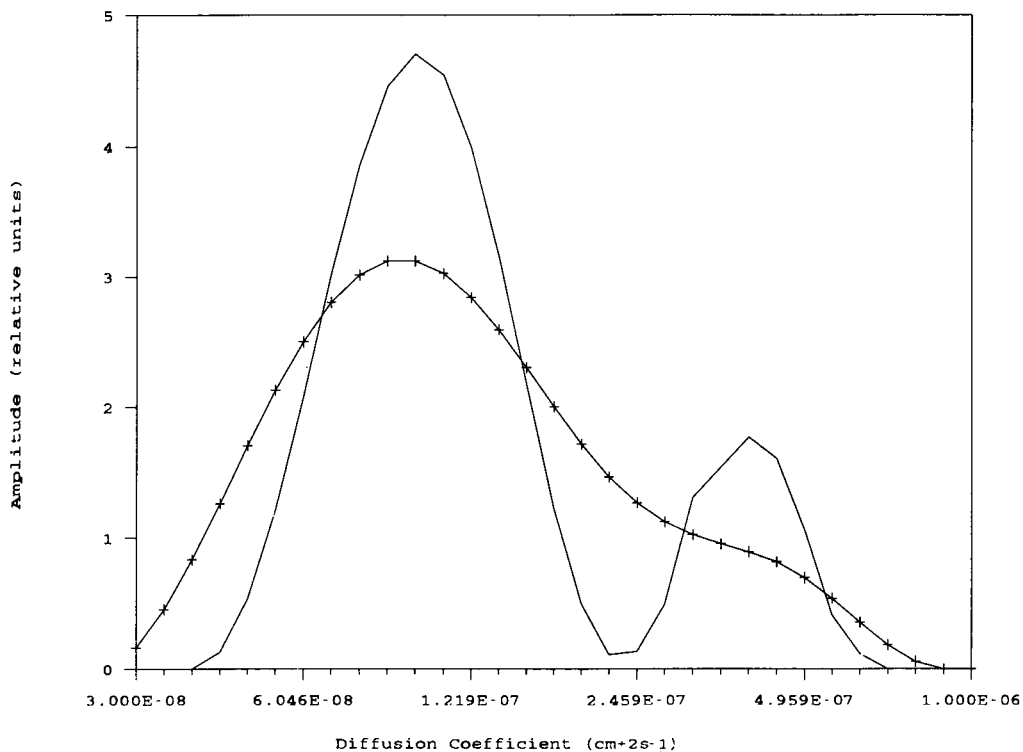


FIGURE 1 Distribution function $F(\Gamma)$ (relative amplitudes in number concentration) calculated from simulated intensity correlation functions, contaminated by different levels of noise: (---) noise level of 0.10%; (- + - + - + -) noise level of 0.22%.

generation of correlators having the facility to space all its points of correlation in a pure geometric series. The delay or sampling time of every channel is derived from the former one by multiplying this former one by a freely chosen but fixed constant, called the delay ratio. In this way a fixed ratio is defined between each two adjacent correlation channels. As an immediate consequence, the successive delay or sampling times, on which the correlation function decay is studied, are not linked in time making correlators of this type not 100% real time machines. The efficiency of these correlators decreases with an increasing number of channels used. Thanks to the decoupling of the sampling time and the sample time in the geometric spacing scheme, the sample time can be chosen much smaller than in the previously described correlators while still covering the same range of correlation. In a 128-channel correlator of this type, a decay range of 100 ms is covered by setting the delay ratio to 1.11 while fixing the sample time to 1 μ s. With this choice of sampling times, the correlation function is well resolved over the whole time range.

Analysis of an autocorrelation function

The determination of the distribution function $F(\Gamma)$, which appears under the integral sign in the right-hand

side of Eq. 5, requires the application of a so-called Laplace inversion to this equation. Due to the fact that experimental data are inherently noisy and extending over a finite time window, an infinitely large number of feasible functions $F(\Gamma)$ can be found which all fit the experimentally measured points to any given accuracy (Phillips, 1962). To make things worse, different feasible functions $F(\Gamma)$ can also differ from each other by any finite amount. These problems find their origin in the so-called ill-conditionedness of the Laplace inversion expressed in the fact that small deviations in the data, for example due to the presence of experimental noise, can induce large deviations in the distribution function $F(\Gamma)$. It is not surprising that the procedure of fitting a continuous or discrete set of exponentials to noisy experimental data in general has a reputation of being extremely difficult (Lanczos, 1957). From this it is clear that "the criterion of the best fit" in any norm (linear, quadratic, maximum ...) is not enough to select the unique and best fitting distribution function $F(\Gamma)$. Indeed, the most probable function may not be the one which best fits the data in the sense of the norm used. A number of different methods using a priori knowledge and other techniques to reconstruct $F(\Gamma)$ from the data are in use today. All of them have their advantages and

disadvantages and none of them give an unbiased solution under all experimental conditions. A nonexhaustive list of methods now follows including a representative reference in the field of photon correlation spectroscopy:

- Fourier transform methods (Gardner et al., 1959),
- Cumulant analysis (Koppel, 1972),
- Transformation-Eigenvalue-Eigenfunction expansion (Provencher, 1976),
- Exponential Sampling method (Ostrowsky et al., 1981),
- Laplace inversion with regularization parameter (Provencher, 1982),
- S-exponential sum method (Nash and King, 1983),
- Linear programming (Zimmerman et al., 1985),
- Maximum Entropy (Livesey et al., 1986),
- Laplace-Padé method (Yeramian and Claverie, 1987).

The Cumulant analysis, the Exponential Sampling method (ExpSam), the earlier cited program CONTIN, and the Maximum Entropy method (MEM) will be discussed in more detail since they will be used in the experimental data analysis section later on.

The cumulant method provides an objective analysis of an experimental autocorrelation function. In the cumulant analysis, the exponential term under the integral sign of Eq. 5 is expanded in a power series, which results in the expression

$$\ln[g^{(1)}(\tau)] = \sum_m K_m(\Gamma) \cdot (-\tau)^m / m!, \quad (6)$$

where the K_i are the different cumulants of the distribution function F . The cumulants K_i can be expressed in terms of the moments μ_j

$$\mu_j = \int F(\Gamma) \cdot (\Gamma - \Gamma_{\text{mean}})^j \cdot d\Gamma \quad (7)$$

of F around Γ_{mean} in the following way

$$K_1 = \mu_1 = \Gamma_{\text{mean}}, K_2 = \mu_2, K_3 = \mu_3, K_4 = (\mu_4 - \mu_2^2). \quad (8)$$

The first cumulant is equal to the z average mean D_z of the diffusion coefficients present in the correlation function. The second and the third cumulant provide a measure for the width of the distribution and its skewness respectively. An infinite number of cumulants is necessary to reconstruct the distribution function unambiguously. Because only a small number of them (up to four maximum) can be calculated with sufficient accuracy, only a rough idea of the distribution function can be obtained. It has been shown that an infinite number of widely different functions $F(\Gamma)$ fit the same values of the first three cumulants (Pusey et al., 1974). As a natural extension of the one exponential model of the cumulant method, a frequently used model for multicom-

ponent correlation functions is the double, triple, Dirzac δ -functions, each with a certain finite amplitudes. Assuming n discrete size classes in the scattering sample the $g^1(t)$ function becomes:

$$g^1(t) = \sum_i A_i \cdot \exp(-\Gamma_i t). \quad (9)$$

The summation extends from 1 to n and the number of unknowns in Eq. 9 is $2n$. Inclusion of an exponential with relaxation $\Gamma_0 = 0$ corresponds to infinitely slow moving or infinitely large particles introducing a constant baseline factor A_0 . This adds one more unknown to Eq. 9. The minimization usually takes place in the χ^2 norm. The main problem is the choice of a good and unbiased set of starting values for the fit. The ill-conditionedness of the fit of exponentials to experimental data is demonstrated by the fact that the surface of minimization is covered with many local minima where the χ^2 number of the fit reaches values close to the one of the global minimum. A bad set of starting values and a poor fitting algorithm may lead to convergence in a local minimum, producing values for the unknowns of the model which can be far away from the values in the global minimum. We have explored some possibilities for the choice of the starting values, which will be considered now:

(a) As a first trial, the first two moments as calculated by the cumulant method can be used to construct the following starting values:

$$\Gamma_1 = \Gamma_{\text{mean}} + \sqrt{\mu_2} \quad \Gamma_2 = \Gamma_{\text{mean}} - \sqrt{\mu_2}. \quad (10)$$

The amplitudes A_1 and A_2 are taken to be equal if no assumptions can be made about their values relative to each other.

(b) A graphical representation of the logarithm of the first-order correlation function can reveal an estimation of the number of discrete components in the correlation function. To get values for the decay rates and amplitudes of each component, one can combine a priori knowledge about the components in the sample and the graphical representation of the correlation function.

(c) To check to what extent the final fitting results depend on the starting values, one or a few unrealistic combinations of starting values should be included. The amplitudes A_i should be chosen such that their sum is equal to the intercept of the correlation function. For each set of starting values, a calculation with and without zero relaxation component Γ_0 should be executed to check for the presence of a baseline A_0 .

CONTIN is based on a least squares fit of the first-order autocorrelation function to a sum of exponentially spaced set of decaying exponentials. Non-negativity of the amplitudes of the distribution function is built in the minimization procedure as a priori constraint.

To suppress artificial oscillations on the calculated distribution function $F(\Gamma)$, a regularizer quantifying the second derivative of $F(\Gamma)$ is simultaneously minimized (Provencher, 1982).

In the exponential sampling method, one makes use of the analytical form of the Eigenvalues and the Eigenfunctions of the integral equation 5 (Ostrowsky et al., 1981). Under mild conditions it is shown that the distribution function $F(\Gamma)$ can be written as a finite sum of exponentially spaced δ functions:

$$F(\ln\Gamma) = \sum a_n \cdot \delta(\ln\Gamma - \ln\Gamma_n) \quad (11)$$

with

$$a_n = (\pi/\omega_{\max}) \cdot F(\ln\Gamma_n). \quad (12)$$

The exponential spacing of the δ functions is set by:

$$\Gamma_{n+1} = \Gamma_n \cdot \exp(\pi/\omega_{\max}). \quad (13)$$

The noise level of the correlation function determines the number of exponential functions in the reconstruction and the value of the parameter ω_{\max} , defining the resolution of the reconstruction. Substituting Eq. 11 into Eq. 5 leads to a simple data reduction procedure in which the amplitudes a_n of the histogram of the distribution function are calculated by a non-negative least square procedure (Lawson and Hanson, 1974).

The Maximum Entropy method is essentially a two-step method (Livesey and Skilling, 1985; Livesey et al., 1986). First, the set of feasible functions $F(\Gamma)$ is constructed by eliminating all functions which do not fit the experimental points to within a certain deviation. The criterion used for this selection is based on the χ^2 test. In the second step the most probable solution is selected by determining in the (still infinitely large) feasible set the distribution function with the highest entropy value. The entropy S is evaluated using the Shannon-Jaynes model

$$S = - \int F(D) \cdot \ln F(D) \cdot dD. \quad (14)$$

This two-step process of reconstruction is known in literature as the "Historic Maximum Entropy method."

MATERIALS AND METHODS

PCS was used to record the intensity autocorrelation of the light scattered by the eye lens of an anaesthetized rabbit *in vivo*. The experimental set-up is identical to the one described by Tanaka and Ishimoto except for the laser light source, an Argon ion laser in our case used at 488 nm and at 5 mW power output (Tanaka and Ishimoto, 1977). The polarization of the laser beam is in the vertical plane. The temperature of the eye lens is taken to be 37°C. The scattering angle was 135°. The correlator used was a 128-channel Brookhaven BI-8000 operated in its geometrically spaced mode. The sample time was chosen to be 2.5 μ s while a constant ratio of 1.24 between the delay

time of each two adjacent channels was introduced. Using 48 channels, the span of the correlation function was 79 ms. One more delay channel was automatically recorded with a sampling time of 109 ms. This means that a range of relaxation rates ranging over five decades can be recorded during one single correlation run. The goniometer and the light collection optics were from ALV (Langen, B.R.D.).

For the analysis of the experimental autocorrelation function gradually more complex techniques were used starting from the cumulant method (Brookhaven ISDA package) over the double and triple exponential model to several methods for calculating a continuous form of the distribution function $F(\Gamma)$. The minimization to the double and triple exponential function according to the χ^2 procedure was carried out by the MINUIT program (D506 from the CERN library). For the continuous forms of distribution functions the CONTIN program, the Exponential Sampling and Maximum Entropy methods have been used. In all three methods, the x -axis of the distribution function was set in a diffusion coefficient scale ranging from $1 \times 10 \exp(-6)$ to $1 \times 10 \exp(-11) \text{ cm}^2 \text{s}^{-1}$ and was sampled on an exponentially spaced grid.

RESULTS AND DISCUSSION

Analysis of the correlation functions

Fig. 2 shows the normalized intensity autocorrelation function $g^2(t)$, as recorded under the circumstances described above. The total accumulation time was 60 s. Table 1 lists the results of the cumulant fit up to the third order of the experimental data from this figure. The upper part of the table shows that the diffusion coefficients, obtained by fitting the experimental correlation function covered by channels 2 to 48, differ from each other to a great extent, depending on the order of the cumulant fit. It is not surprising that the χ^2 values, indicating the overall quality of the fit, are high and change significantly according to the order of the cumulants fitted.

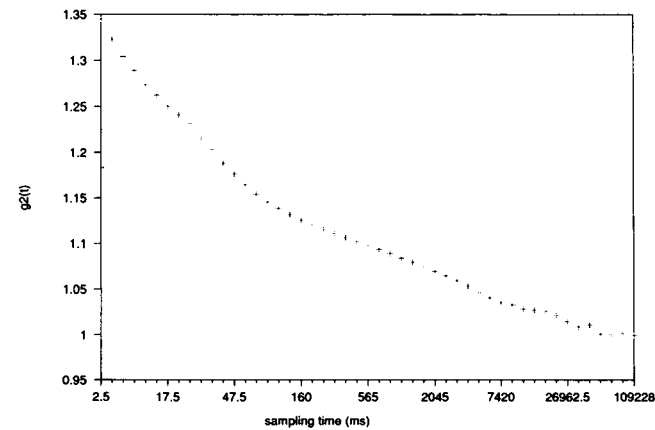


FIGURE 2 Experimental normalized intensity autocorrelation function $g^2(t)$ on a logarithmic time scale ranging from 2.5 μ s to 109.228 ms.

TABLE 1 Cumulant analysis up to third order to the correlation function of Fig. 2

Channels	Order	$D_z [\times 10^{-9} \cdot \text{cm}^2 \cdot \text{s}^{-1}]$	μ_2/Γ^2	skewness	$\chi^2 (\times 10^{-1})$
2 ↓ 48	1	0.08			8.19
	2	1.16	0.23		2.63
	3	0.12	-33.7	112.6	1.19
Channels 2 ↓ 10	Order	$D_z [\times 10^{-7} \cdot \text{cm}^2 \cdot \text{s}^{-1}]$	μ_2/Γ^2	Skewness	$\chi^2 (\times 10^{-5})$
	1	0.80			2.52
	2	0.94	0.89		2.07
	3	0.89	0.25	4.47	2.48

A more stable result is obtained by fitting only the first part of the correlation function (channels 2–10, covering a time scale up to 27.5 μs). The much lower and more constant value of the χ^2 fit as a function of the order of the cumulant fit indicates that a mono-exponential model is adequate for this first part of the correlation function (see the lower part of Table 1). Because this part of $g^2(t)$ corresponds to the fastest decaying relaxation time present in the scattering sample, and considering the fact the α -crystallin is responsible for over 85% of the total scattering potential of the mammalian eye lens, it is assumed that this first decay component can be assigned to the diffusion of individual α -crystallin molecules. The value of the diffusion coefficient for the α -crystallins in the eye lens *in vivo* as found by cumulants however, is ~ 2.5 times lower than the diffusion coefficient of the same molecules in a highly diluted solution (Andries and Clauwaert, 1985). This decrease is attributed to the diffusion hindering presence of a high concentration of α -crystallins as well as the β - and γ -crystallins. As a consequence, a more complicated model for the fitting of the autocorrelation function is recommended.

Fig. 3 shows the logarithm of the first-order autocorrelation function as calculated from the second-order function in some more detail on a shorter time scale. Curve A shows the correlation function on a linear time scale up to 120 μs while part B shows the same correlation function on the longer time scale up to 14 ms. This figure clearly suggests the presence of several relaxation processes in the eye lens with quite different relaxation times.

From these graphs the most obvious model for the form of the autocorrelation is the finite sum of discrete exponentials. Starting values for the different fits were obtained in the following way.

For the double exponential model of distribution, the first set of starting values was generated from the results of the cumulants fit:

$$\Gamma_1 = \Gamma_{\text{mean}} + \sqrt{\mu_2} \quad \Gamma_2 = \Gamma_{\text{mean}} - \sqrt{\mu_2}. \quad (15)$$

Because the α -crystallin molecules give by far the largest contribution in the scattered intensity, the autocorrelation function will contain a decay component with a diffusion coefficient of $\sim 2.5 \times 10^{-7} \text{ cm}^2 \cdot \text{s}^{-1}$, as calculated by earlier measurements (Andries and Clau-

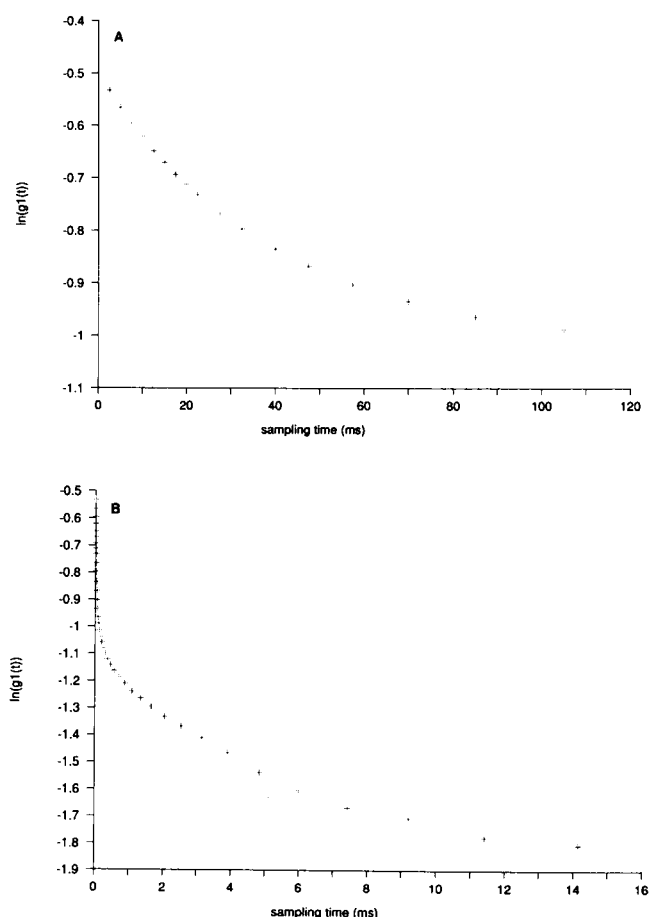


FIGURE 3 Logarithm of the normalized field autocorrelation function $g^1(t)$ resulting from the intensity correlation function of Fig. 2; two time scales are covered: (A) a linear time scale from 0 to 120 μs ; (B) a linear time scale from 0 to 14 ms.

waert, 1985). From curve A in Fig. 3 one can derive for the second component a decay constant which is ~ 100 times smaller. From graphical extrapolation, the amplitude of the slower decaying component is chosen twice as large as the one of the faster decay, so that the following values were used as a starting point for the fit:

$$\begin{aligned}A_1 &= 0.20 \quad A_2 = 0.40 \\ \Gamma_1 &= 2.5 \times 10 \exp (+4)s^{-1} \\ \Gamma_2 &= 2.5 \times 10 \exp (+2)s^{-1}. \end{aligned}\quad (16)$$

For a third set of starting values, the amplitudes and diffusion coefficients are chosen equal:

$$A_1 = A_2 = 0.30 \quad \Gamma_1 = \Gamma_2 = 2.5 \times 10 \exp (+4)s^{-1}. \quad (17)$$

Plausible starting values for the triple exponential model of distribution function were obtained using the following strategies. We accept once again that the main contribution from the scattering capacity of the eye lens proteins comes from the α -crystallin. A second decay process with a diffusion coefficient about 10 times smaller originates from long distance heterogeneities in the scattering power due to the well known size polydispersity of the α -crystallin (Pusey and Tough, 1985). Inspection of curve B in Fig. 3 reveals the presence of a third, long time relaxation process with a diffusion coefficient about 10 times smaller, situated at $\sim 2.5 \times 10 \exp (-9) \text{ cm}^2\text{s}^{-1}$. Graphical extrapolation yields an equal

amplitude for both two slower components, who combined are twice the amplitude of the faster decay.

Thus, we start the fit with the following values:

$$\begin{aligned}A_1 = A_2 = A_3 &= 0.20 \quad \Gamma_1 = 2.5 \times 10 \exp (+4)s^{-1} \\ \Gamma_2 &= 2.5 \times 10 \exp (+3)s^{-1} \\ \Gamma_3 &= 2.5 \times 10 \exp (+4)2^{-1}. \end{aligned}\quad (18)$$

To check the dependence of the final results of the starting values for this model of the distribution function, we choose equal amplitudes and decay constants for all three components:

$$A_1 = A_2 = A_3 = 0.20$$

$$\cdot \Gamma_1 = \Gamma_2 = \Gamma_3 = 2.5 \times 10 \exp (+4)s^{-1}. \quad (19)$$

For each set of starting values a calculation with and without constant baseline component A_0 is executed. The results of the fits to two and three exponential terms are summarized in Tables 2 and 3, respectively.

The different sets of starting values for the diffusion coefficients, given in the former section, all converge to the same final values indicating that, with the algorithm used, a stable fit could be obtained for two and three decaying exponentially decaying components with or without the addition of a baseline A_0 . In the fits without a baseline, the constant background in the correlation function seems to be absorbed into the smaller relaxation component lowering its value significantly compared with the fits where a baseline has been included.

TABLE 2 Double exponential fit: $g^{(1)}(\tau) = A_0 + A_1 \cdot \exp(-\Gamma_1\tau) + A_2 \cdot \exp(-\Gamma_2\tau)$

conditions I						
	A_0	A_1	$D_1(\text{cm}^2/\text{s})$	A_2	$D_2(\text{cm}^2/\text{s})$	χ^2
starting values	0	0.20	2.63×10^{-9}	0.20	0.22×10^{-9}	
final values	0	0.25	2.16×10^{-9}	0.33	0.80×10^{-9}	0.33×10^{-2}
starting values	0.20	0.20	2.63×10^{-9}	0.20	0.22×10^{-9}	
final values	0.12	0.25	2.42×10^{-7}	0.19	1.86×10^{-9}	0.38×10^{-4}
conditions II						
	A_0	A_1	$D_1(\text{cm}^2/\text{s})$	A_2	$D_2(\text{cm}^2/\text{s})$	χ^2
starting values	0	0.20	2.50×10^{-7}	0.40	2.50×10^{-9}	
final values	0	0.25	2.16×10^{-7}	0.33	0.80×10^{-9}	0.33×10^{-2}
starting values	0.20	0.20	2.50×10^{-7}	0.20	2.50×10^{-9}	
final values	0.12	0.25	2.42×10^{-7}	0.23	1.85×10^{-9}	0.38×10^{-4}
conditions III						
	A_0	A_1	$D_1(\text{cm}^2/\text{s})$	A_2	$D_2(\text{cm}^2/\text{s})$	χ^2
starting values	0	0.30	2.50×10^{-7}	0.30	2.50×10^{-7}	
final values	0	0.25	2.16×10^{-7}	0.33	0.80×10^{-9}	0.33×10^{-2}
starting values	0.20	0.20	2.50×10^{-7}	0.20	2.50×10^{-7}	
resulting values	0.12	0.25	2.42×10^{-7}	0.23	1.83×10^{-9}	0.38×10^{-4}

TABLE 3 Triple exponential fit: $g^{(1)}(\tau) = A_0 + A_1 \cdot \exp(-\Gamma_1\tau) + A_2 \cdot \exp(-\Gamma_2\tau) + A_3 \cdot \exp(-\Gamma_3\tau)$

conditions I							
	A_0	A_1	$D_1(cm^2/s)$	A_2	$D_2(cm^2/s)$	A_3	$D_3(cm^2/s)$
starting values	0	0.20	2.50×10^{-7}	0.20	2.50×10^{-8}	0.20	2.50×10^{-9}
final values	0	0.23	2.90×10^{-7}	0.12	7.88×10^{-8}	0.25	0.27×10^{-9}
starting values	0.15	0.15	2.50×10^{-7}	0.15	2.50×10^{-8}	0.15	2.50×10^{-9}
final values	0.05	0.23	2.99×10^{-7}	0.11	1.02×10^{-8}	0.21	0.45×10^{-9}
conditions II							
	A_0	A_1	$D_1(cm^2/s)$	A_2	$D_2(cm^2/s)$	A_3	$D_3(cm^2/s)$
starting values	0	0.20	2.50×10^{-7}	0.20	2.50×10^{-7}	0.20	2.50×10^{-7}
final values	0	0.23	2.90×10^{-7}	0.12	7.87×10^{-9}	0.25	0.25×10^{-9}
starting values	0.15	0.15	2.50×10^{-7}	0.15	2.50×10^{-7}	0.15	2.50×10^{-7}
final values	0.05	0.23	2.99×10^{-7}	0.11	1.01×10^{-8}	0.21	0.45×10^{-9}

In the fits with a baseline the final values for the unknown parameters show that the triple exponential model for the correlation function can be regarded as an extension of its double exponential counterpart. The amplitude and the value of the largest diffusion coefficient are nearly unchanged in both fits while the second component in the double exponential fit is split up in two components. This can be seen by comparing the values of the amplitudes and the diffusion coefficients in both fits. The value of the amplitudes of the residuals of both models, shown relative to each other in Fig. 5, indicate that a triple exponential function is a better model for the field correlation function than the double exponential function. Fits to a distribution function with more than three δ functions were not executed since this would raise the number of independent parameters of the model unreasonably high as compared with the signal-to-noise ratio expected for the correlation function (Bertero et al., 1982; Bertero et al., 1984).

Up till now in studies of this kind, most authors have used a double exponential fit for the analysis of autocorrelation functions resulting from a dynamic light scattering experiments on eye lenses in vivo (Delaye et al., 1982; Libondi et al., 1986; Benedek et al., 1987; Bursell et al., 1989). This choice was obvious for several reasons. For a long time now, it is accepted that the increase in scattering of the incoming light in older and cataractous lenses is due to the presence of a large scattering units in the eye lens cytoplasm (Benedek, 1971). As a consequence one could look for two relaxation components representing two size classes in the autocorrelation function. The first component found is then associated with the α crystallin which forms the predominant fraction in the total scattering intensity in healthy lenses. To explain the increase in light scattering in cataractous lenses a second scattering unit with at least one dimension in the order of the wavelength of the laser light λ

used, was looked for. In most cases, the decay of the correlation function was investigated deliberately on two time scales, based on this idea. A short time range up to $\sim 200 \mu s$ was chosen for covering the fast diffusion of the individual α crystallins while a longer range in the order of 20 ms looked for the presence of particles with large dimensions up to 1,000 nm (Bursell et al., 1989). As only a correlator with linearly spaced channels was available, the correlation functions for both time scales were recorded separately and spliced together afterwards to obtain one function containing both relaxation processes. This operation, however, is unfavorable because it introduces an additional amount of noise. From Fig. 3 B, which shows the correlation function recorded in this study on a linear time scale, the double exponential model indeed seems to represent the maximum of information that can safely be extracted. The use of a logarithmic correlator gives equivalent resolution on both time scales while avoiding the need for splicing two or more separately recorded correlation functions.

Apart from fitting of the autocorrelation function to a model of discrete δ functions, a semi-continuous histogram model has been applied. This was suggested by the fact that at least the α crystallins carry a size heterogeneity of $\sim 10\%$ so that a δ function with zero width for the diffusion coefficient is an underestimation of reality (Licinio and Delaye, 1988). The optimization of the histogram of δ functions to the experimental data has been worked out by the CONTIN, Exponential Sampling, and Maximum Entropy method.

The distribution functions, calculated by each of the three methods, are shown in Fig. 4. As this figure clearly shows, all three methods give results which are quite comparable to each other. They suggest four separate populations of relaxations with diffusion coefficients in the range of $3 \times 10 \exp(-7)$, $3 \times 10 \exp(-8)$, $3 \times 10 \exp(-9)$, and $1 \times 10 \exp(-10) \text{ cm}^2 \text{s}^{-1}$, respectively.

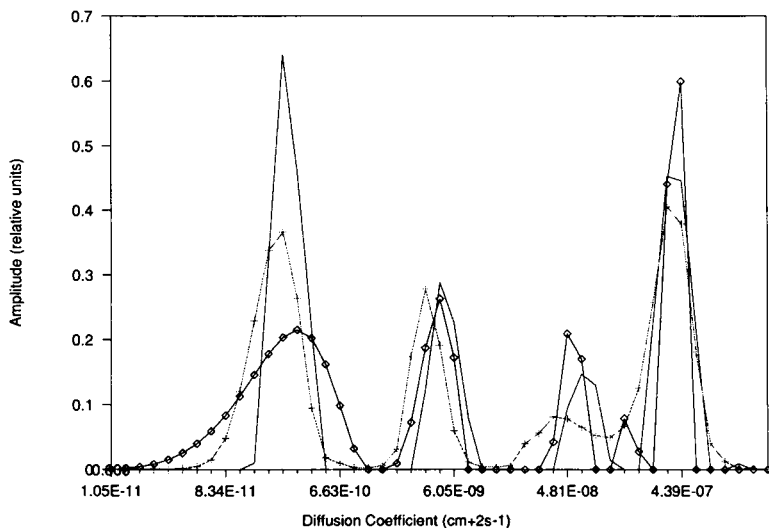


FIGURE 4 Distribution function $F(\Gamma)$ (relative amplitudes in number concentration), calculated from the experimental correlation function of Fig. 2, using a semi-continuous histogram model; the histogram has been fitted to the experimental data using the following method: (---) the Exponential Sampling technique; (- + - + - + -) the Maximum Entropy technique; (- ◊ - ◊ - ◊ - ◊ -) the CONTIN method.

Selection of the optimal fitting procedure

To choose between the different models for the correlation function, we have been looking for an objective criterion to compare the different fitting procedures. We consider a method of analysis as the best one when the

deviations between the experimental and calculated values are smaller than in any other method and when the deviations are randomly distributed around zero on the complete time scale of the correlation function.

The residuals of the double and triple exponential fit and of the CONTIN method are shown in Fig. 5. The Exponential Sampling and Maximum Entropy method

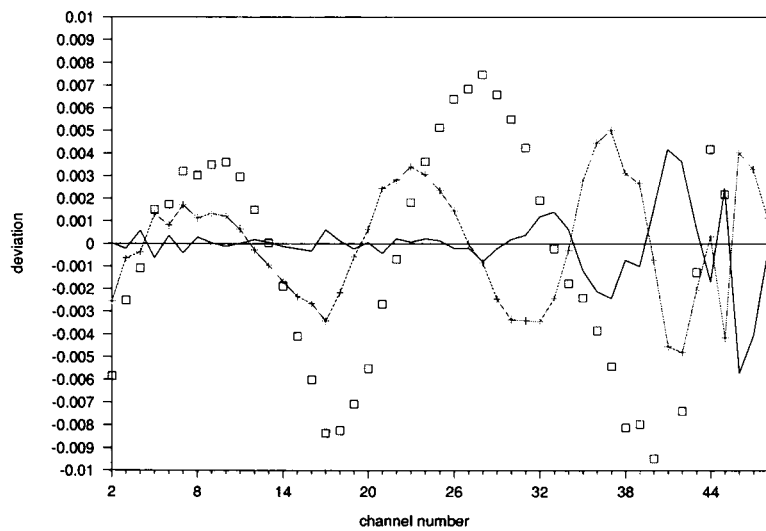


FIGURE 5 The residual differences (deviation) between the model correlation function and the experimental correlation function at each point (channel number) of the correlation function: (---) model correlation function obtained with the CONTIN method; (- + - + - + -) the triple exponential fit, including a base line A_0 ; (□ □ □ □) the double exponential fit, including a base line A_0 .

gave residuals which were comparable to those of CONTIN.

It is clear from this figure that the methods which fit a histogram to the correlation function perform much better to our criterion than those based on a δ function approach for the distribution function. Only at higher channel numbers, related to sampling times larger than 10 ms, the deviations are larger and in the same order of magnitude as for the triple exponential model. These deviations are related to the lower signal-to-noise ratio at these long delay times as can be seen in Fig. 2.

From this we can conclude that in our experimental conditions, the distribution function as calculated by the histogram methods can reliably be interpreted for analytical and diagnostic purposes up to diffusion coefficients larger than $1 \times 10 \exp(-9) \text{ cm}^2\text{s}^{-1}$. From this the three populations of relaxation processes can unambiguously be distinguished while the presence and mainly the position of the fourth very slow population is questionable.

The smallest three relaxation rates are similar to those present in a highly concentrated solution of isolated α -crystallin (Licinio et al., 1987). This similarity is not surprising since, as already cited, the α -crystallin molecules are responsible for over 85% of the total scattering intensity in the eye lens. The fourth component showing up in our work probably only exists under *in vivo* conditions although the logarithmic correlator used in this work is better suited for registering such a slow relaxation process.

The identification of the "particles" responsible for the scattering can be based on the results of the isolated α -crystallin solutions.

The largest diffusion component is associated to the mutual diffusion of the α crystallins in the eye lens cytoplasm. The second component with a diffusion coefficient of $\sim 3 \times 10 \exp(-8) \text{ cm}^2\text{s}^{-1}$ arises from self-diffusion due to size (and charge) heterogeneity of the crystallins (Pusey and Tough, 1985). The identification of the other components is speculative. For α -crystallin solutions (Licinio et al., 1987), it has been proposed that the third peak is related to the motion of reversibly formed clusters of crystalline molecules. The fourth component has been related to structural relaxations which are supposed to take place in highly concentrated glassy colloidal systems.

CONCLUSION

The measuring conditions for an *in vivo* light scattering study of the mammalian eye lens for clinical and

diagnostic purposes are unfavorable: only short measuring times and a low primary laser flux are allowed in order not to damage the components of the eye.

By choosing the proper light scattering conditions and making use of a logarithmic correlator, we have been able to record correlation functions *in vivo* of such a quality that a detailed analysis is possible and justified. The correlation functions are best analyzed by fitting a semi-continuous histogram to the distribution function. Three different methods which calculated the distribution function in this way all gave comparable results. Four relaxation processes could be discerned in the experimental correlation function. A high degree of similarity has been noticed between the scattering spectrum and the relaxation rates of a highly concentrated solution of isolated α -crystallin and *in vivo* measurements on a complete and intact eye lens.

We have shown that the technique of Photon Correlation Spectroscopy is a valuable tool for quantitative routine diagnostic research on the mammalian eye lens. It has been shown that the formation of certain types of cataract (e.g., the widely spread senile type) is associated with the occurrence of aggregates (built up from the naturally present smaller scattering units). The growth of these aggregates can be studied by PCS in their natural environment over a time period of years by this safe and noninvasive type of measurement. A decrease in the amplitude of the relaxation process, associated with the decay of the α -crystallin molecules and a simultaneous increase in the amplitude of the larger scattering components, as compared over several measurements each separated in time, may indicate the onset of these types of cataract.

The sensitivity of the method allows it to be used as an important analytical technique in the study of prevention and treatment of cataract. The authors suggest a routine medical examination of this type, taking only a few minutes per patient (the analysis of the correlation function included) to be performed on a large scale on a regular time basis. The results of the analysis should be stored in a database by electronic means to be able to compare the results immediately with all former recorded data.

We thank Stijn De Kerpel for a careful reading of the manuscript and many helpful suggestions. We also thank the reviewers for their comments on the manuscript. It is a pleasure to thank Dr. P. Licinio for the interesting and stimulating discussions on the subject of *in vivo* light scattering and for analyzing our experimental data with the Maximum Entropy method.

We also thank the National Fund for Scientific Research (Belgium) and the Fund for Medical Research (Belgium) for financial support. This research was performed within the framework of the European

Community Concerted Action on Cellular Aging and Disease (EURAGE).

Received for publication 19 April 1990 and in final form 1 October 1990.

REFERENCES

- Andries, C., and J. Clauwaert. 1985. Photon correlation spectroscopy and light scattering of eye lens proteins at high concentrations. *Biophys. J.* 47:591–605.
- Benedek, G. B. 1971. Theory of transparency of the eye. *Appl. Optics.* 10:459–73.
- Benedek, G. B., L. T. Chylack Jr., T. Libondi, P. Magnante, and M. Pennett. 1987. Quantitative detection of the molecular changes associated with early cataractogenesis in the living human lens using quasi-elastic light scattering. *Curr. Eye Res.* 6:1421–32.
- Berne, B. J., and R. Pecora. 1976. *Dynamic Light Scattering*. John Wiley and Sons, Inc., New York. 376 pp.
- Bertero, M., P. Boccaci, and E. R. Pike. 1982. On the recovery and resolution of exponential relaxation rates from experimental data. I. A singular-value analysis of the Laplace transform inversion in the presence of noise. *Proc. R. Soc. Lond. A.* 383:15–29.
- Bertero, M., P. Boccaci, and E. R. Pike. 1984. On the recovery and resolution of exponential relaxation rates from experimental data. II. The optimum choice of experimental sampling points for Laplace transform inversion. *Proc. R. Soc. Lond. A.* 393:51–65.
- Bursell, S.-E., R. S. Baker, J. N. Weiss, J. F. Haughton, and L. I. Rand. 1989. Clinical photon correlation spectroscopy evaluation of human diabetic lenses. *Exp. Eye Res.* 49:241–258.
- Chu, B. 1974. *Laser Light Scattering*. Academic Press, New York. 317 pp.
- Delaye, M., J. I. Clark, and G. B. Benedek. 1982. Identification of the scattering elements responsible for lens opacification in cold cataract. *Biophys. J.* 37:647–656.
- Delaye, M., and A. Tardieu. 1983. Short-range order of crystallin proteins accounts for lens transparency. *Nature (Lond.)*. 302:415–417.
- Gardner, D. G., J. C. Gardner, G. Laush, and W. W. Meinke. 1959. Method for the analysis of multicomponent exponential decay curves. *J. Chem. Phys.* 31:978–986.
- Koppel, D. 1972. Analysis of macromolecular polydispersity in intensity correlation spectroscopy: the method of cumulants. *J. Chem. Phys.* 57:4814–4820.
- Lanczos, C. 1957. *Applied Analysis*. Prentice-Hall Inc., Englewood Cliffs, NJ. 272–280.
- Lawson, C. L., and R. J. Hanson. 1974. *Solving Least Squares Problems*. Prentice-Hall Inc., Englewood Cliffs, NJ. 340 pp.
- Libondi, T., P. Magnante, L. T. Chylack, Jr., and G. B. Benedek. 1986. In vivo measurement of the aging rabbit lens using quasielastic light scattering. *Curr. Eye Res.* 6:411–419.
- Licinio, P., M. Delaye, A. K. Livesey, and L. Léger. 1987. Colloid dispersions of α -crystallin proteins. II. Dynamics: a maximum entropy analysis of photon correlation spectroscopy data. *J. Physique.* 48:1217–1223.
- Licinio, P., and M. Delaye. 1988. Direct and hydrodynamic interactions between α -crystallin proteins in dilute colloidal dispersions: a light scattering study. *J. Colloid Interface Sci.* 123:105–116.
- Livesey, A. K., and J. Skilling. 1985. Maximum entropy theory. *Acta Crystallogr. Sect. B. Struct. Crystallogr. Cryst. Chem.* 41:113–122.
- Livesey, A. K., P. Licinio, and M. Delaye. 1986. Maximum entropy analysis of quasielastic light scattering from colloidal dispersions. *J. Chem. Phys.* 84:5102–5107.
- Nash, P. J., and T. A. King. 1983. Analysis of photon correlation spectral decay curves by the S-exponential sum method. *J. Chem. Soc. Faraday Trans. II* 79:989–1009.
- Ostrowsky, N., D. Sornette, P. Parker, and E. R. Pike. 1981. Exponential sampling method for light scattering polydispersity analysis. *Optica Acta.* 28:1059–1070.
- Phillips, D. L. 1962. A technique for the numerical solution of certain integral equations of the first kind. *J. Assoc. Comput. Mach.* 9:84–97.
- Provencher, S. W. 1976. A Fourier method for the analysis of exponential decay curves. *Biophys. J.* 16:27–41.
- Provencher, S. W. 1982. A constrained regularization method for inverting data represented by linear algebraic or integral equations. *Comput. Phys. Commun.* 27:213–227, 229–242.
- Pusey, P. N., D. E. Koppel, D. W. Schaefer, R. D. Camerini-Otero, and S. H. Koenig. 1974. Intensity fluctuation spectroscopy of laser light scattered by solutions of spherical viruses. *Biochemistry.* 13:952–960.
- Pusey, P. N., and R. J. A. Tough. 1985. Particle interactions. In *Dynamic Light Scattering*. R. Pecora, editor. Plenum Publishing Corporation, New York. 85–179.
- Schulz-Dubois, E. O. 1983. High-Resolution intensity interferometry by photon correlation. In *Photon Correlation Techniques in Fluid Mechanics*. E. O. Schulz-Dubois, editor. Springer-Verlag, Heidelberg. 6–30.
- Tanaka, T., and C. Ishimoto. 1977. In vivo observation of protein diffusivity in rabbit lenses. *Invest. Ophthalmol.* 16:135–140.
- Yeramian, E., and P. Claverie. 1987. Analysis of multiexponential functions without a hypothesis as to the number of components. *Nature (Lond.)*. 326:169–174.
- Zimmerman, K., M. Delaye, and P. Licinio. 1985. Analysis of multiexponential decay by a linear programming method: application to light scattering spectroscopy. *J. Chem. Phys.* 82:2228–2235.